PHYSICAL REVIEW A **69**, 063415 (2004)

Asymmetry of above-threshold ionization of metal clusters in two-color laser fields: A time-dependent density-functional study

H. S. Nguyen* and A. D. Bandrauk
Laboratoire de Chimie Théorique, Faculté des Sciences, Université de Sherbrooke, Sherbrooke, Quebec J1K 2R1, Canada

C. A. Ullrich
Department of Physics, University of Missouri–Rolla, Rolla, Missouri 65409, USA
(Received 5 May 2003; published 24 June 2004)

Above threshold ionization (ATI) spectra of small metal clusters (e.g., Na_4 and Na_4^+) are calculated numerically using a spherical jellium model and time-dependent density functional theory for two-color (1064 and 532 nm) ultrashort (25 fs) laser pulses as a function of phase difference between the two fields. ATI spectra and ionized electron fluxes are obtained in the two opposite directions of the linearly polarized laser fields. The asymmetry, defined as the difference in electron yield, is shown to depend strongly on the carrier-envelope phase of the second-harmonic (2ω) field. The ATI spectra allow one to identify the range of kinetic energies of the ionized electrons where the asymmetry mainly occurs. Comparisons are made between calculations with and without self-interaction correction and also with previous exact numerical solutions of the one-electron systems H and H_2^+ [A. D. Bandrauk and S. Chelkowski, Phys. Rev. Lett. **84**, 3562 (2000)] where such asymmetry effects had first been observed. We find that ATI spectra in the clusters generally have much longer energy plateaus than in previously studied one-electron systems, with cutoffs up to 30–40 times the ponderomotive energy U_p. In high-harmonic generation spectra, on the other hand, no extended plateaus are observed.

DOI: 10.1103/PhysRevA.69.063415 PACS number(s): 32.80.Rm, 31.15.Ew, 36.40.Gk, 42.50.Hz

I. INTRODUCTION

Laser control of electronic and nuclear motion has become a growing area of research [1] due to the availability of laser pulses with variable and controllable amplitudes and phases even in the ultrashort ($t<10$ fs) and intense ($I \geqslant 10^{14}$ W/cm^2) regime, thanks to steady progress in laser technology [2]. Controlling electrons in atoms has had considerable success by manipulating the phase difference between two laser fields. In particular, the $\omega+2\omega$ scenario, i.e., the simple superposition of a field of frequency ω and its second harmonic, with total field

$$E(t) = E_0(t)[\cos(\omega t) + f\cos(2\omega t + \phi)], \qquad (1)$$

where $E_0(t)$ is the field envelope, ϕ the relative phase, and f the relative amplitude, permits control of the angular distribution of photoelectrons in atomic ionization processes [3] or directional control of photocurrents in quantum wells [4]. Quantum wells can be viewed as simple analogs of molecular systems, and electron-nuclear photodissociation-ionization yield asymmetries have been observed already in the molecule HD, with possible applications to isotope separation [5]. Possible applications of coherent control with intense ultrashort pulses have recently been suggested from numerical simulations for the generation of attosecond pulses and even for the measurement of laser pulse phases [6,7].

On the theoretical side, the first observations of such electron-nuclear asymmetric yields were made from numerical solution of the time-dependent Schrödinger equation (TDSE) for the one-electron H_2^+ molecule [8,9], for which exact non-Born-Oppenheimer simulations can be performed in one dimension with current supercomputers. Exact three dimensional (3D) simulations of the two-electron H_2 system with static nuclei (Born-Oppenheimer) have recently been carried out [10]. Extension of such simulations to multielectron systems is of great interest, but can only be achieved by replacing the multidimensional TDSE with effective single-electron theories such as density functional theory (DFT) [11] and its extension to the time-dependent regime, TDDFT [12].

In this work, we use TDDFT methods to investigate the electron dynamics of small Na clusters in intense fields. The electron dynamics of Na clusters has been widely studied within the jellium model [13–15], using the local density approximation (TDLDA) with and without self-interaction correction (SIC). The conclusion was that TDLDA and TDLDA-SIC give similar results [16] for observables such as ionization rates and high-harmonic generation (HHG) spectra. Further tests of the SIC employing more realistic molecular models beyond jellium confirmed this conclusion [17]. In these studies, SIC was implemented using an accurate single local potential scheme based on the time-dependent version [18] of the optimized effective potential method of Krieger, Li, and Iafrate (KLI) [19]. This KLI-SIC approach has been shown to give adequate descriptions of dynamical properties in the regime of strong excitations [16,17].

In the present paper, we will study the open-shell clusters Na_4 and Na_4^+ using the local spin-density approximation (LSD) with and without KLI-SIC. We will in particular focus on calculating ATI spectra and ionized electron fluxes in the two opposite directions along the linearly polarized laser

*Deceased (November 2002).

fields. Our primary motivation is to demonstrate that TDDFT methods can reproduce the essential physics of intense laser field coherent control in many-electron systems, obtained in our previous simulations for one-electron systems such as H and H_2^+ [6–9]. It will emerge that metallic clusters show very similar features as previously observed in atoms, i.e., ATI spectra with extensive plateaus, and pronounced left-right asymmetries as a function of phase in two-color lasers fields.

The standard quasistatic tunneling model [2,20,21], which very successfully describes strong-field laser-atom interactions, turns out to be adequate for HHG spectra in clusters, but substantially underestimates the cutoff of the ATI plateaus. This indicates fundamental differences between the nonlinear electron dynamics in metal clusters and in one- or two-electron atoms and molecules.

In our calculations, we will treat the valence electrons exactly in a 3D TDDFT approach, whereas core electrons are represented in a spherical jellium model. In reality, the shape of Na_4 and Na_4^+ is strongly prolate rather than spherical [22], even though at room temperature ($k_BT=0.025$ eV) small alkali metal clusters are "fluxional," i.e., they have no fixed geometry due to a large number of near isoenergetic conformations [23]. However, since the purpose of the present paper is to demonstrate a fundamental strong-field effect of the delocalized valence electrons, we will for simplicity ignore all details of the ionic structure. As we will argue below, the effects that we study here (ATI and HHG) are likely to persist even in the nonspherical case. Furthermore, at high laser intensities the spectral differences between spherical and deformed cluster models become more and more washed out due to power broadening [24].

This paper is organized as follows. In Sec. II we give a brief summary of the TDDFT formalism applied to open-shell clusters in the jellium model, explaining the LSD and KLI-SIC approaches. Section III provides some details of our numerical method and of the observables of interest. In Section IV we present and discuss our numerical results, and we conclude in Sec. V. We use Hartree atomic units unless otherwise indicated.

II. TDDFT FOR SPHERICAL METAL CLUSTERS

Our investigations are based on the jellium model [13–15], which treats the valence electrons explicitly and the inner core as a uniform, spherical, positive charge background with radius $R=r_sZ^{1/3}$, where $r_s=4$ a.u. is the Wigner-Seitz radius of bulk sodium, and Z is the number of ions. The associated electrostatic potential seen by the valence electrons is given by

$$v_{\rm jel}(r)=\begin{cases} -Z/r, & r>R, \\ Zr^2/2R^3-3Z/2R, & r<R. \end{cases} \tag{2}$$

The time-dependent Kohn-Sham (TDKS) equations for the single-particle valence spin orbitals $\varphi_{j\sigma}(\mathbf{r},t)$ are given by

$$i\frac{\partial}{\partial t}\varphi_{j\sigma}(\mathbf{r},t)=\left(-\frac{\nabla^2}{2}+v_\sigma[n_\uparrow,n_\downarrow](\mathbf{r},t)\right)\varphi_{j\sigma}(\mathbf{r},t), \tag{3}$$

where the total density is

$$n(\mathbf{r},t)=\sum_{\sigma=\uparrow,\downarrow}n_\sigma(\mathbf{r},t)=\sum_\sigma\sum_{j=1}^{N_\sigma}f_{j\sigma}|\varphi_{j\sigma}(\mathbf{r},t)|^2. \tag{4}$$

To treat open-shell clusters, we introduce occupation numbers $f_{j\sigma}$, normalized as $N_\sigma=\Sigma_j f_{j\sigma}$. In ground state calculations, we employ the usual procedure of assigning equal, fractional occupation numbers to degenerate orbitals. For example, the Na_4^+ cluster has three valence electrons, two spin-up and one spin-down. The $1s\uparrow$ and $1s\downarrow$ orbitals each contain one electron, and the $1p_0\uparrow$, $1p_{+1}\uparrow$ and $1p_{-1}\uparrow$ orbitals are each occupied by $1/3$ of an electron [25]. The resulting total ground-state density n and spin densities n_σ are therefore spherical for Na_4^+ and all other open- or closed-shell clusters (provided the jellium background is spherical). Once the cluster is excited by the laser field, the occupations of the $1p$ orbitals will no longer remain identical because their different orientations with respect to the laser polarization cause the orbitals to ionize at different rates.

The TDKS effective spin-dependent potential v_σ is the sum of external, Hartree, and exchange-correlation (xc) time-dependent potentials,

$$v_\sigma[n_\uparrow,n_\downarrow](\mathbf{r},t)=v_{\rm ext}(\mathbf{r},t)+\int d^3r'\frac{n(\mathbf{r}',t)}{|\mathbf{r}-\mathbf{r}'|}+v_{{\rm xc}\sigma}[n_\uparrow,n_\downarrow](\mathbf{r},t), \tag{5}$$

where

$$v_{\rm ext}(\mathbf{r},t)=v_{\rm jel}(r)+E(t)z, \tag{6}$$

and $E(t)$ is defined in Eq. (1) for two colors.

The simplest approximation is to use static xc potentials such as the LSD, with the density $n(\mathbf{r},t)$ obtained from the time-dependent orbitals $\varphi_{j\sigma}(\mathbf{r},t)$, i.e.,

$$v_{{\rm xc}\sigma}^{\rm LSD}[n_\uparrow,n_\downarrow](\mathbf{r},t)=\left.\frac{de_{\rm xc}^h(\bar{n}_\uparrow,\bar{n}_\downarrow)}{d\bar{n}_\sigma}\right|_{\bar{n}_{\uparrow,\downarrow}=n_{\uparrow,\downarrow}(\mathbf{r},t)}. \tag{7}$$

For the xc energy density of a spin-polarized homogeneous electron gas, $e_{\rm xc}^h$, we use the following standard expression [26]:

$$e_{\rm xc}^h(n,\xi)=e_{\rm xc}^h(n,0)+[e_{\rm xc}^h(n,1)-e_{\rm xc}^h(n,0)]f(\xi), \tag{8}$$

where $n=n_\uparrow+n_\downarrow$, $\xi=(n_\uparrow-n_\downarrow)/n$, and

$$f(\xi)=\frac{(1+\xi)^{4/3}+(1-\xi)^{4/3}-2}{2(2^{1/3}-1)}. \tag{9}$$

Explicit expressions for $e_{\rm xc}^h(n,0)$ and $e_{\rm xc}^h(n,1)$ can be found in Ref. [27]. We use here the correlation energy density in the parametrization of Vosko *et al.* [28].

In order to perform a self-interaction correction (SIC) using a *single* local potential, one can arrive variationally [18] at a spin-dependent optimized effective potential akin to the static KLI method [19]:

$$v_{\mathrm{xc}\sigma}^{\mathrm{KLI}}(\mathbf{r},t)=\sum_j \frac{n_{j\sigma}(\mathbf{r},t)}{n_\sigma(\mathbf{r},t)}\Bigg\{u_{\mathrm{xc}j\sigma}^{\mathrm{SIC}}(\mathbf{r},t) + \int d^3r'|\varphi_{j\sigma}(\mathbf{r}',t)|^2[v_{\mathrm{xc}\sigma}^{\mathrm{KLI}}(\mathbf{r}',t)-u_{\mathrm{xc}j\sigma}^{\mathrm{SIC}}(\mathbf{r}',t)]\Bigg\}, \tag{10}$$

$$u_{\mathrm{xc}j\sigma}^{\mathrm{SIC}}(\mathbf{r},t)=v_{\mathrm{xc}\sigma}^{\mathrm{LSD}}[n_\uparrow,n_\downarrow](\mathbf{r},t)-v_{\mathrm{H}}[n_{j\sigma}](\mathbf{r},t)-v_{\mathrm{xc}\sigma}^{\mathrm{LSD}}[n_{j\sigma},0](\mathbf{r},t). \tag{11}$$

We note that the u's in Eqs. (10) and (11) contain the appropriate subtraction of orbital self-interaction. Furthermore, Eq. (10) is an integral equation for the effective local xc potential which is easily solved at each time step [17–19]. To summarize this formal discussion, we have at our disposal two different, spin-dependent local effective potentials which contain exchange and correlation, $v_{\mathrm{xc}\sigma}^{\mathrm{LSD}}$, Eq. (7), and $v_{\mathrm{xc}\sigma}^{\mathrm{KLI}}$, Eq. (10), which can be used in the TDKS equation (3). Previous model TDDFT calculations of atomic clusters in intense laser fields used only the Hartree potential $v_{\mathrm{H}}(\mathbf{r},t)$ [29] or $v_{\mathrm{x}\sigma}^{\mathrm{KLI}}$ with no correlation and SIC [30] for 1D arrays of atoms.

III. NUMERICAL METHOD

To calculate above-threshold ionization (ATI) spectra, we adapt to our 3D calculations the method described by Pohl *et al.* [31]. The kinetic energy spectrum of the ionized electrons is computed from the local frequency spectrum of the single electron wave functions $\varphi_{j\sigma}(\mathbf{r}_{\mathrm{b}},t)$ at a point $\mathbf{r}_{\mathrm{b}}$ near the grid boundary and sufficiently far from the cluster in order to make Coulomb effects negligible. Absorbing boundary conditions between $\mathbf{r}_{\mathrm{b}}$ and the grid boundaries guarantee that only outgoing waves are collected over time t and then Fourier transformed to give the total kinetic energy distribution in forward and backward direction as

$$n(E)=\sum_{\sigma=\uparrow,\downarrow}\sum_{j=1}^{N_\sigma}|\varphi_{j\sigma}(\mathbf{r}_{\mathrm{b}},E)|^2. \tag{12}$$

In our calculations we assume cylindrical symmetry due to the presence of linearly polarized radiation, and we therefore use a two-dimensional grid $\mathbf{r}=(z,\rho)$ as in our previous exact H_2^+ calculations [32]. We record electron wave functions $\varphi_{j\sigma}$ at two opposite points on the z axis at $\mathbf{r}_\pm=(\pm z_{\mathrm{b}},0)$, where z_{b} is about $0.75z_{\max}$, $z_{\max}$ being the grid size (see below). Our simulations also allow for measuring the ionization signal in a cone (forward and backward) within an angle θ in order to detect total asymmetries which can even be used in principle to measure absolute phases of ultrashort intense pulses [7,33]. We thus define the total probability flux passing the surface at z_{b},

$$P_{\mathrm{b}}(t)=2\pi\int_0^t d\tau\int_0^{\rho_0} j(z_{\mathrm{b}},\rho,t)\rho d\rho, \tag{13}$$

where the local flux is given as

$$j(z_{\mathrm{b}},\rho,t)=\mathrm{Im}\sum_{\sigma,j}\left[\varphi_{j\sigma}^*\frac{\partial}{\partial z}\varphi_{j\sigma}\right]_{z=z_{\mathrm{b}}}, \tag{14}$$

and $\rho_0=z_{\max}\tan\theta$.

The numerical simulations were performed for a two-color laser field with intensity $I_1=6\times10^{12}$ W/cm^2 at $\lambda_1=1064$ nm ($\omega=1.16$ eV) and $I_2=1.5\times10^{12}$ W/cm^2 at $\lambda_2=532$ nm ($2\omega=2.32$ eV). The angle $\theta=15°$ was chosen as in our previous work [7,33] as an experimentally feasible collection angle of ionized electrons with respect to the laser polarization direction. Both pulses (ω and 2ω) were assumed to have the same Gaussian envelope with full width at half maximum length (duration) 25 fs.

The chosen laser intensities and wavelengths determine certain essential physical parameters which allow for quasistatic interpretations of strong field laser-atom processes [2,20,21]. One is the ponderomotive energy $U_p=eI/4m\omega^2$ which for $\omega=1.16$ eV is $U_p(\omega)=0.56$ eV and $U_p(2\omega)=0.035$ eV. This allows for defining the Keldysh parameter γ separating tunneling and multiphoton ionization regimes for an ionization potential I_p:

$$\gamma=\sqrt{I_p/2U_p}=\begin{cases}1.5 & (\mathrm{Na}_4),\\ 2.1 & (\mathrm{Na}_4^+).\end{cases} \tag{15}$$

The tunneling ionization regime is defined by $\gamma<1$, so that the present parameters situate our calculations near and above the limit of this regime. In the multiphoton regime, considering ionization as direct transitions, we can identify the minimal photon number n_s for ionization, which is given by

$$n_s=I_p/\omega=\begin{cases}3 & (\mathrm{Na}_4),\\ 5 & (\mathrm{Na}_4^+).\end{cases} \tag{16}$$

Finally, we calculate the maximum spatial amplitude of the laser induced electron oscillations:

$$\alpha=\frac{eE}{m\omega^2}=\begin{cases}7.0\ \text{a.u.} & (\omega),\\ 0.875\ \text{a.u.} & (2\omega).\end{cases} \tag{17}$$

The larger value, 7 a.u., determines the minimum grid size. We choose $z_{\max}=62.5$ a.u. to insure sufficient space for the laser induced oscillations after ionization. Thus z_{b} is at 47.5 a.u., followed by an absorbing boundary of width 15 a.u. to minimize reflections. Along the r direction, we have $r_{\max}=35$ a.u. and an absorbing boundary of width 10 a.u. Convergence of the spectra (ATI as well as HHG) was verified by varying the grid size between 50×25 a.u. and 62.5×35 a.u.

IV. RESULTS AND DISCUSSION

We first tabulate in Tables I and II the total energies and KS orbital eigenvalues for our Na_4 and Na_4^+ jellium cluster models, obtained by solving the time-independent KS equations corresponding to the TDKS equations (3). We find that correlation generally lowers the total energy E_{tot} and the various orbital energies. The SIC within the KLI scheme has a large stabilizing effect on the inner valence orbital $1s\downarrow$ in

TABLE I. Total ground-state energy E_{tot} and orbital energy eigenvalues of the $1s\uparrow$, $1p\uparrow$, and $1s\downarrow$ orbitals for Na_4 (in eV), obtained for a spherical jellium model with different DFT approaches.

	E_{tot}	$1s\uparrow$	$1p\uparrow$	$1s\downarrow$
LSD (x only)	−46.53	−3.76	−2.16	−2.78
KLI-SIC (x only)	−47.35	−4.39	−2.79	−5.34
LSD	−49.80	−4.34	−2.64	−3.83
KLI-SIC	−48.98	−4.69	−2.98	−5.92

both clusters. On the other hand, SIC stabilizes the $1s\uparrow$ and $1p\uparrow$ orbitals only in Na_4, whereas in Na_4^+ the effect is reversed. Thus the presence of the extra electron in Na_4 ($1s^2 1p^2$) as compared to Na_4^+ ($1s^2 1p^1$) results in a somewhat increased ionization potential $I_p = 2.98$ eV for Na_4 and a decreased ionization potential $I_p = 5.41$ eV for Na_4^+ when the KLI-SIC method is used.

It is to be noted that these ionization potentials (which we take to be the negative of the HOMO $1p\uparrow$, i.e., the highest occupied molecular orbital, in keeping with KLI-SIC results [34]) are somewhat lower than previous *ab initio* molecular values calculated at equilibrium geometries. Thus $I_p(Na_4) = 4.4$ eV and $I_p(Na_4^+) = 8.2$ eV were reported using pseudopotential LSD calculations [35]. These numbers are to be compared to the atomic ionization potential, $I_p(Na) = 5.14$ eV. We emphasize that our lower I_p's are due to the use of a spherical jellium model for the core, which can be viewed as simulating the average geometry of the clusters expected at room temperature, whereas the *ab initio* molecular geometries correspond to zero-temperature equilibrium structures. One expects that at higher temperatures, geometries dilate and randomize, thus lowering I_p's.

We illustrate in Fig. 1(a) the two pulses which are superposed with changing relative phases ϕ to give net resulting fields $E(t)$ [see Eq. (1)], for the cases $\phi = 0$ [Fig. 1(b)], $\phi = \pi/4$ [Fig. 1(c)], and $\phi = \pi/2$ [Fig. 1(d)]. In the limit of a few cycles of ω ($\sim$5 fs pulse width), Fig. 1(b) becomes similar to a single-frequency "cos" pulse, whereas Fig. 1(d) approaches a single-frequency "sin" pulse. These ultrashort single-frequency pulses have recently been shown to give rise to very large ionization asymmetries from which we can infer the absolute phase of these pulses [33]. We note that in the $\omega + 2\omega$ coherent superpositions illustrated in Fig. 1, the phase $\phi = 0$ superposition [Fig. 1(b)] exhibits the largest electric field asymmetry since the relative maximum field amplitudes are $E_1/E_2 = \sqrt{I_1/I_2} = 2$ [9]. The $\phi = \pi/2$ superposition [Fig. 1(d)] has local maxima and minima of equal absolute amplitude strength, but one notes that locally the fields are

TABLE II. Same as in Table I, for Na_4^+.

	E_{tot}	$1s\uparrow$	$1p\uparrow$	$1s\downarrow$
LSD (x only)	−51.70	−7.38	−5.51	−6.75
KLI-SIC (x only)	−51.16	−7.00	−5.14	−9.39
LSD	−54.97	−8.06	−6.08	−7.73
KLI-SIC	−52.79	−7.37	−5.41	−9.93

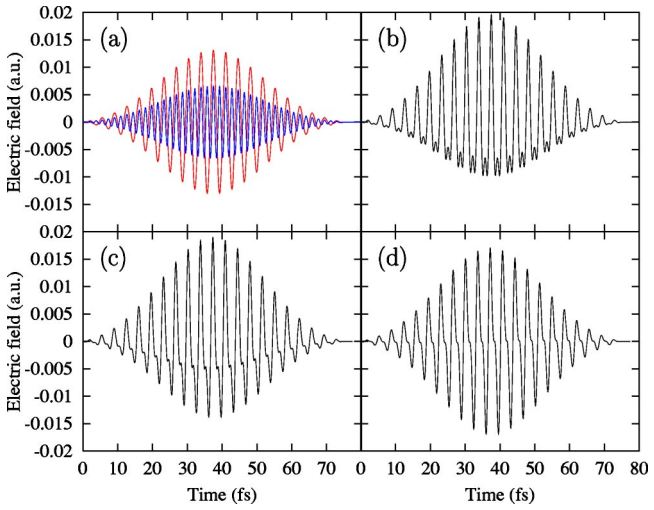

FIG. 1. (a) Electric fields $E_1(t)$ and $E_2(t)$ associated with a two-color 25-fs laser pulse: $\lambda_1 = 1064$ nm, $\lambda_2 = 532$ nm, $I_1 = 6 \times 10^{12}$ W/cm^2, $I_2 = I_1/4$, and relative phase $\phi = 0$. (b)–(d) Resulting net field $E(t)$ [see Eq. (1)] for $\phi = 0$, $\phi = \pi/4$, and $\phi = \pi/2$, respectively.

asymmetric due to the presence of a "kink" between the positive and negative amplitudes. As shown for the 1D single-electron system H_2^+, this results in large asymmetries of the ionized electrons and dissociated protons, which have the unusual feature that bare protons and electrons preferentially move in the *same* direction, which we have called "counter-intuitive" [7,33]. In the following, we examine whether similar phenomena exist in sodium clusters and present our results based on the TDDFT approach outlined above.

Figure 2(a) illustrates the ATI spectra of Na_4, obtained with KLI-SIC for single-color excitation at $\lambda = 1064$ nm, $I = 6 \times 10^{12}$ W/cm^2, and pulse duration 25 fs. Both left and right ionization patterns are nearly identical, with slight differences reflecting nonadiabatic excitations from ultrashort pulses [7]. In particular, notice that the ATI spectrum is nearly constant up to $E_{max} = 15\omega \approx 30U_p$, where U_p is the ponderomotive energy defined in the previous section. Quasistatic tunneling ionization models of single-electron atoms predict $E_{max} = 10U_p$ [20,34]. In the case of extended molecules, we have shown previously that collisions with neighboring ions can raise this up to $12U_p$, thus extending high-order harmonic generation plateaus beyond the atomic maximum $E_{max} = I_p + 3.17U_p$ [36]. This has been confirmed in simulations of chains of atoms [29]. Thus the single-color ATI spectrum of Na_4 clearly shows an unusually long plateau with a cutoff (sharp decrease) around $E_{max} = 30U_p$. The same phenomenon is observed for the Na_4^+ cluster, see Fig. 3(a), the main difference being the slightly lower intensity as there is one less $1p$ valence electron in this case. In summary, one-color excitation of both Na_4 and Na_4^+ results in extended ATI spectra with cutoffs at around $30U_p$, which far exceeds the single-electron atom cutoff of $10U_p$.

We next return to the Na_4 ATI spectra illustrated in Figs. 2(b)–2(f)) with the two-color coherent superposition $E(t)$, see Eq. (1) and Fig. 1. At $\phi = 0$ where the positive field amplitude is twice the negative amplitude or, equivalently,

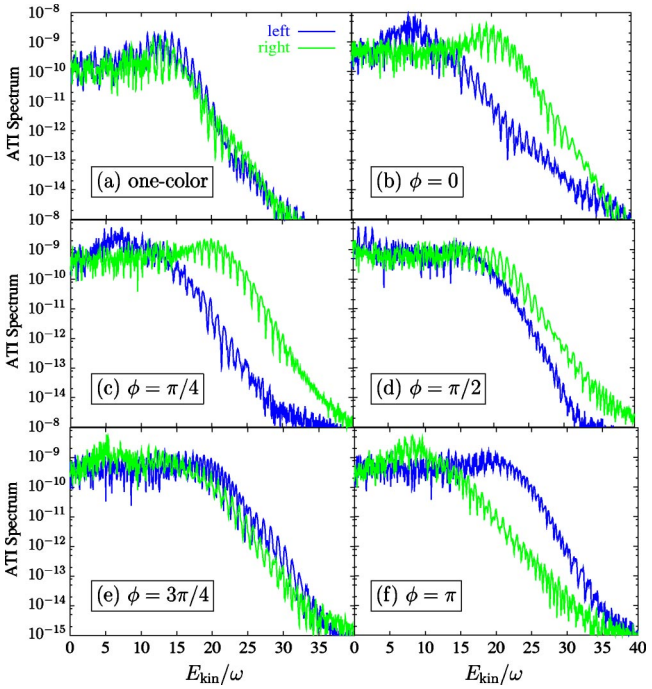

FIG. 2. ATI spectra of a Na_4 jellium cluster, calculated with KLI-SIC. (a) Single-color excitation; (b)–(f) two-color excitations with varying relative phase ϕ, as indicated.

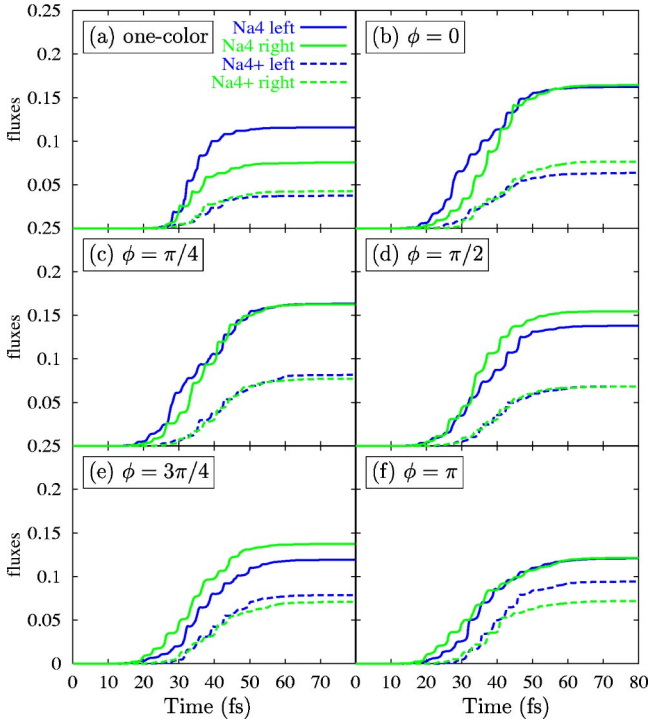

FIG. 4. Left and right probability fluxes $P_b(t)$ [Eq. (13)] for Na_4 and Na_4^+, calculated with KLI-SIC.

maximum intensities have the ratio 4:1, the left and right ATI spectra exhibit different cutoffs. Thus the left-ionized electrons have a cutoff at $E_{max} \approx 12\omega = 22U_p$, whereas the right-ionized electron cutoff is at $E_{max} \approx 22\omega = 40U_p$, i.e., a ratio of approximately 2:1. Furthermore, one must emphasize an anomaly, akin to the counterintuitive processes found previously in H_2^+ [7,33], i.e., there is a preponderance after $E \approx 15\omega \approx 30U_p$ of electrons ionized in the right direction in spite of the fact that the net field, see Fig. 1(b), is overwhelmingly *positive*. This effect is further confirmed at $\phi = \pi$ relative phase difference in Fig. 2(f). The same "counterintuitive" effect occurs in Na_4^+ [Fig. 3(f)], albeit again with slightly less intensity since there is one electron less in the $1p$ HOMO orbital.

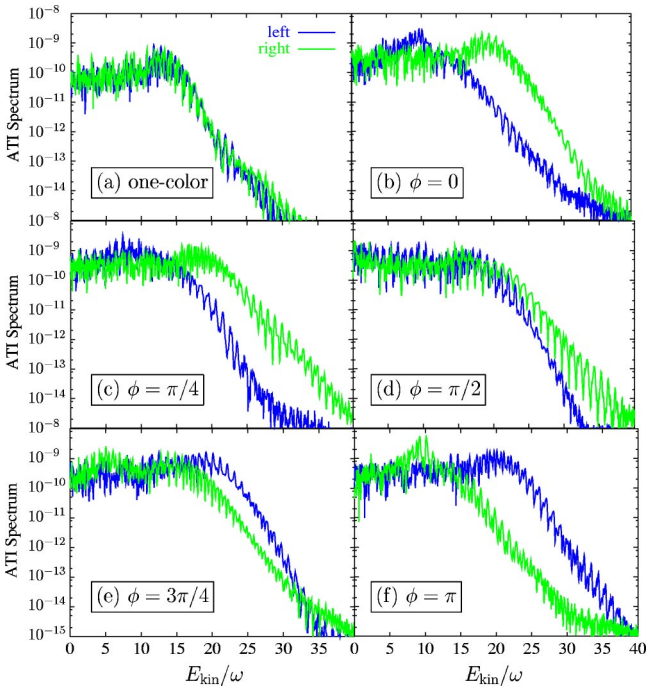

FIG. 3. Same as Fig. 2, for Na_4^+.

On examining the $\phi = \pi/2$ or "sin" coherent superposition of the two fields ω and 2ω, one observes that for both Na_4 and Na_4^+ [Figs. 2(d) and 3(d)] the ATI energy cutoff has been extended with respect to the single field excitation to $E_{max} \approx 40U_p$. For the case of both clusters, the $\phi = \pi/2$ or "sin" field superposition produces less asymmetry in the ATI spectra, reflecting the fact that the maximum-minimum field amplitudes are more symmetric in time.

The ATI spectra displayed in Figs. 2 and 3 were calculated with a TDKS approach using the KLI-SIC xc potential. We have found that very similar spectra are obtained using the LSD xc potential. It thus appears that, qualitatively, self-interaction corrections have only very little effect on the kinetic-energy spectra of the ionized electrons. This is not too surprising, since SIC is most effective for localized orbitals, whereas the features of ATI are determined by continuum states.

The difference between LSD and KLI-SIC becomes more apparent when we look at an integrated time-dependent quantity such as the total time-dependent flux according to Eq. (13). The results are summarized for Na_4 and Na_4^+ and the two computational schemes in Fig. 4 (KLI-SIC) and Fig. 5 (LSD). Each panel shows the left and right flux associated with one-color ionization [Figs. 4(a) and 5(a)] and two-color coherent field superposition for various phases [Figs.

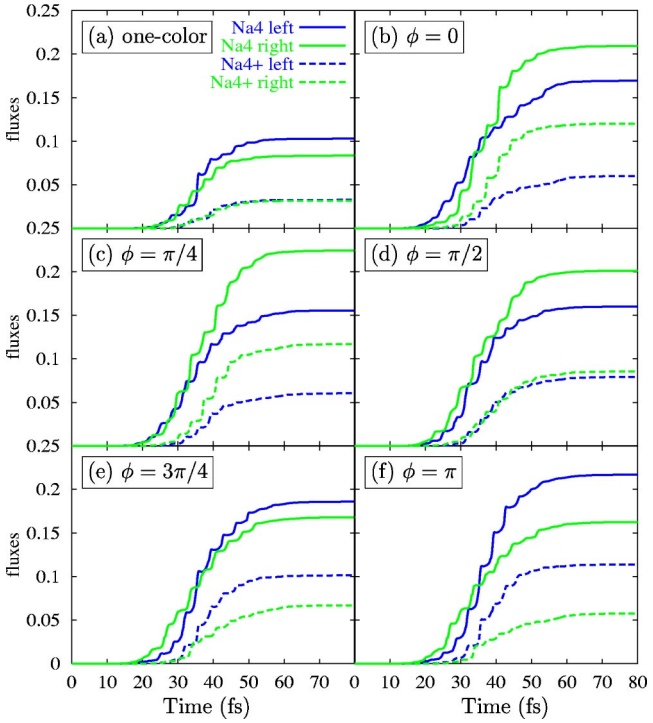

FIG. 5. Same as Fig. 4, calculated with LSD.

4(b)–4(f) and 5(b)–5(f)]. The general patterns of ionization of Na_4 and Na_4^+ follow similar trends in both KLI-SIC and LSD, where, as expected, the flux associated with Na_4^+ is smaller, due to the larger binding energy of the valence electrons caused by the positive charge state of the system.

However, some interesting features can be observed in the details of the left-right asymmetries of the ionization fluxes. For one-color ionization [Figs. 4(a) and 5(a)], the net flux asymmetries are very small for Na_4^+, but are appreciable for Na_4. This somewhat surprising observation reflects the nonadiabatic excitation with ultrashort laser pulses, and appears more pronounced in KLI-SIC than in LSD. In both cases, the left signal is stronger, which can be explained by an asymmetry induced during the switching-on of the laser pulse: the first cycle starts off with an electric field in the positive direction.

For the two-color excitations, the left-right asymmetry is very pronounced in LSD. From Fig. 5 we see that maximum asymmetry occurs at $\phi=0$ and $\pi/4$, and with reversed direction at $\phi=\pi$. At $\phi=\pi/2$, the asymmetry is only small. Notice that the asymmetry is again "counterintuitive": for example, at $\phi=0$, the flux is predominantly to the right, whereas the net field is mainly positive, see Fig. 1(b). At $\phi=3\pi/4$ and $\phi=\pi$, the field is more negative and electrons now again follow counterintuitively, this time to the left, in the direction of the negative field. We will discuss the physical reasons of this anomalous behavior below.

For Na_4^+, the left-right asymmetry under two-color excitations shows the same behavior in KLI-SIC (Fig. 4) as in LSD (Fig. 5), although somewhat less pronounced. For Na_4, on the other hand, it appears to be almost absent in KLI-SIC in some cases, such as $\phi=0$. This can be explained by a competition between the "intuitive" asymmetry due to the

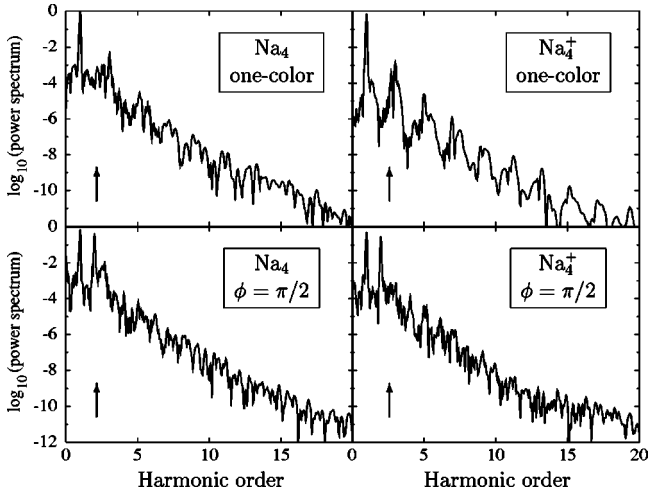

FIG. 6. HHG spectra for Na_4 and Na_4^+, calculated with LSD, for one- and two-color (phase $\phi=\pi/2$) excitations. The arrows indicate the positions of the Mie plasmon energies.

nonadiabatic excitation [see the discussion of Figs. 4(a) and 5(a) above] and the "counterintuitive" asymmetry, which in these cases seem to have about equal magnitude and thus cancel each other.

Next, we discuss harmonic generation. Figure 6 shows HHG spectra for our spherical model of Na_4 and Na_4^+, calculated with LSD (KLI-SIC gives very similar results). We compare the cases of one-color and two-color excitation, the latter with relative phase $\phi=\pi/2$. The quasiclassical model for HHG predicts cutoffs at $E_{max}=I_p+3.17U_p$, which corresponds to harmonic orders 4 and 7 for Na_4 and Na_4^+, respectively. The HHG spectra in Fig. 6 show hardly any indication for plateaus beyond the third harmonic, but instead decrease more or less continuously.

We note that the collective Mie plasmon energies [13,14] for Na_4 and Na_4^+ are 2.54 and 3.02 eV, i.e., between the second ($2\omega=2.32$ eV) and third ($3\omega=3.48$ eV) harmonics. In Fig. 6, the HHG cutoffs thus appear to be set by the Mie plasmons, whose tails absorb most of the oscillator strength beyond the third harmonic. The dominating nature of the Mie plasmon in the linear and nonlinear dipole response of metal clusters is well known [15] (plasmon energies can be obtained as the field-free oscillation frequencies of the initially displaced valence electron cloud). However, we point out that collective plasmon effects are an unlikely cause for the large extent of the ATI plateaus observed in Figs. 2 and 3. As a check, we performed calculations for Na clusters with noninteracting valence electrons and found ATI spectra with very similar cutoffs.

We conclude this discussion with some remarks concerning validity and limitations of the spherical jellium model. As we have explained before, at or above room temperature one should consider an average of the various possible ionic configurations of the cluster. One might wonder whether the resulting averaged ionic background is robust under the influence of strong laser fields. For the time scales of interest in this paper, this is indeed the case. We study here electron dynamics following excitation by 25-fs laser pulses, and propagate up to 80 fs. This is very short compared to typical

time scales for ionic dynamics (a few picoseconds) [15].

On the other hand, spherical averaging of ionic configurations becomes less well-justified at lower temperatures, and eventually one needs to consider the explicit ionic positions of the minimum conformations. To predict the signatures of the transition from the high- to the low-temperature regime in ATI spectra and fluxes thus requires the use of pseudopotentials [37], which is beyond the scope of the present approach. However, the pronounced asymmetry of the ATI spectra is likely to persist even in the nonspherical case, see the case of H_2 and H_2^+. Furthermore, the valence electrons are delocalized not only in jellium, but also in a real Na_4 or Na_4^+ molecule. Collective effects and power broadening at high laser intensities will therefore still play an important role, even in the low-temperature case.

V. CONCLUSION

We have presented ATI spectra for Na_4 and Na_4^+ clusters in a two-color excitation scheme using a spherical jellium model for core electrons and TDDFT for the valence electrons. In both cases we observe strong phase dependence of the asymmetries of the ionization yields reflected in the calculated ATI spectra and probability fluxes passing through the grid boundaries. The asymmetries are maximal for the relative phase difference $0<\phi<\pi/2$ between the two-color (ω and 2ω) fields. In the one-color excitation, ATI energies up to 30 U_p are obtained. In the two-color excitation scheme, right and left electrons have cutoffs (maxima) in ATI energies at 40 and 20 U_p, respectively, suggesting a transfer of energy of $\sim 20U_p$ between the two directions. In the case of previous calculations on one-electron systems [8,9] similar asymmetries were found but the maximum ATI energy never exceeded 3 U_p. This suggests that different ionization mechanisms occur in the clusters.

The ionization asymmetries discovered in the one-electron systems H and H_2^+ [8,9] were found to be "counterintuitive," i.e., nonclassical, and were explained in terms of quasistatic tunneling [20] through the field induced quasistatic barrier at the peaks of the field amplitude. The asymmetries calculated in the present paper also exhibit similar "counterintuitive" behavior. Thus, as seen in Figs. 2(b), 2(c), 3(b), and 3(c), the highest energy electrons ($\sim 40U_p$) are mainly ionized to the right, in the direction of maximum positive field, see Figs. 1(b) and 1(c), contrary to classical response theory. In the clusters the asymmetry disappears around $\phi=3\pi/4$, whereas in the one-electron systems the asymmetry reverses around $\pi/4$, thus reflecting the multielectron character of the clusters.

The present TDDFT approach shows that the energetics of the ionized electrons, as represented by the ATI spectra, Figs. 1 and 3, are similar for LSD and KLI-SIC. The main difference between the two methods is observed in the calculated fluxes, Figs. 4 and 5, thus reflecting the difference in ionization potentials by the two methods (Tables I and II). Our calculations therefore confirm the persistence of counterintuitive, i.e., nonclassical, ionization asymmetries when clusters are exposed to coherent superpositions of short intense laser pulses. The new finding is that this counterintuitive asymmetric ionization results in unusually high-energy ATI spectra, with a ratio of the left and right maximum energies up to 2:1. At the same time, HHG spectra, calculated by the same methods and laser conditions described above, show no high energy plateaus but have cutoffs below the $3.17U_p$ predicted by single electron recollision models [20].

This points to several fundamental differences between atoms and metal clusters in their ionization dynamics under short intense laser pulses. Valence electrons in metal clusters are much more weakly bound, and are delocalized over the entire ionic (or jellium) background, with a high density of states. The electron dynamics thus shows pronounced collective or plasmon effects. As a consequence, multiphoton ionization in clusters typically takes place at intensities 1 to 2 orders of magnitude lower than in atoms. The associated Keldysh parameters are thus in the range $\gamma>1$, which means that ionization occurs in the multiphoton and not in the tunneling regime. This may explain why the quasistatic tunneling model is unable to account for the unusually large extent of the ATI plateaus in metal clusters.

ACKNOWLEDGMENTS

Acknowledgment is made to the donors of the Petroleum Research Fund, administered by the ACS, as well as to the University of Missouri Research Board, for partial support of this research.

[1] M. Shapiro and P. W. Brumer, *Principles of Quantum Control of Molecular Processes* (Wiley-Interscience, New York, 2003).
[2] T. Brabec and F. Krausz, Rev. Mod. Phys. **72**, 545 (2000).
[3] D. W. Schumacher and P. H. Bucksbaum, Phys. Rev. A **54**, 4271 (1996).
[4] E. Dupont, P. B. Corkum, H. C. Liu, M. Buchanan, and Z. R. Wasilewski, Phys. Rev. Lett. **74**, 3596 (1995).
[5] B. Sheehy, B. Walker, and L. F. Di Mauro, Phys. Rev. Lett. **74**, 4799 (1995).
[6] A. D. Bandrauk and H. S. Nguyen, Phys. Rev. A **66**, 031401 (2002).
[7] A. D. Bandrauk, S. Chelkowski, and H. S. Nguyen, Phys. Rev. Lett. **89** 283903 (2002).
[8] A. D. Bandrauk and S. Chelkowski, Phys. Rev. Lett. **84**, 3562 (2000).
[9] S. Chelkowski, M. Zamojski, and A. D. Bandrauk, Phys. Rev. A **63**, 023409 (2001).
[10] K. Harumiya, H. Kono, Y. Fujimura, I. Kawata, and A. D. Bandrauk, Phys. Rev. A **66**, 043403 (2002).
[11] P. Hohenberg and W. Kohn, Phys. Rev. **136**, B864 (1964); W. Kohn and L. J. Sham, Phys. Rev. **140**, A1133 (1965); W. Kohn, Rev. Mod. Phys. **71**, 1253 (1999).
[12] E. Runge and E. K. U. Gross, Phys. Rev. Lett. **52**, 997 (1984); E. K. U. Gross, J. F. Dobson, and M. Petersilka, in *Density*

Functional Theory II, Topics in Current Chemistry Vol. 181 (Springer, Berlin, 1996), p. 81.
[13] W. A. de Heer, Rev. Mod. Phys. **65**, 611 (1993).
[14] M. Brack, Rev. Mod. Phys. **65**, 677 (1993).
[15] F. Calvayrac, P.-G. Reinhard, E. Suraud, and C. A. Ullrich, Phys. Rep. **337**, 493 (2000).
[16] C. A. Ullrich, P.-G. Reinhard, and E. Suraud, J. Phys. B **30**, 5043 (1997); **31**, 1871 (1998).
[17] C. A. Ullrich, P.-G. Reinhard, and E. Suraud, Phys. Rev. A **62**, 053202 (2000).
[18] C. A. Ullrich, U. J. Gossmann, and E. K. U. Gross, Phys. Rev. Lett. **74**, 872 (1995).
[19] J. B. Krieger, Y. Li, and G. J. Iafrate, Phys. Rev. A **45**, 101 (1992).
[20] P. B. Corkum, Phys. Rev. Lett. **71**, 1994 (1993).
[21] A. Scrinzi, M. Geissler, and T. Brabec, Phys. Rev. Lett. **83**, 706 (1999).
[22] V. Bonacic-Koutecky, P. Fantucci, and J. Koutecki, J. Chem. Phys. **93**, 3802 (1990); J. Chem. Rev. **91**, 1035 (1991); J. Chem. Phys. **104**, 1427 (1996).
[23] *Ab initio* quantum chemical calculations [K. Mishima, K. Yamashita, and A. D. Bandrauk, J. Phys. Chem. A **102**, 3157 (1998)] show that Na_4^+ has three minimum energy geometries, triangular (C_{2v}), diamond (D_{2h}) (rhombohedral), and tetrahedral (D_{2d}), separated by very low energy barriers: D_{2h} and D_{2d} lie at −0.017 and 0.062 eV relative to C_{2v}, with transition states at 0.014 eV (between C_{2v} and D_{2h}) and 0.063 eV (between D_{2h} and D_{2d}).
[24] F. Calvayrac, P.-G. Reinhard, and E. Suraud, Phys. Rev. B **52**, R17056 (1995).
[25] The appropriate orbital quantum numbers for a spherical jellium cluster are those of a 3D harmonic oscillator, which differ from those of a spherical atom, see Ref. [13]. The lowest orbitals for jellium clusters are 1*s* and 1*p*.
[26] U. von Barth and L. Hedin, J. Phys. C **5**, 1629 (1972).
[27] R. M. Dreizler and E. K. U. Gross, *Density Functional Theory* (Springer, Berlin, 1990).
[28] S. H. Vosko, L. Wilk, and M. Nusair, Can. J. Phys. **58**, 1200 (1980).
[29] V. Véniard, R. Taïeb, and A. Maquet, Phys. Rev. A **60**, 3952 (1999).
[30] V. Véniard, R. Taïeb, and A. Maquet, Phys. Rev. A **65**, 013202 (2001).
[31] A. Pohl, P.-G. Reinhard, and E. Suraud, Phys. Rev. Lett. **84**, 5090 (2000); J. Phys. B **34**, 4969 (2001).
[32] T. Zuo and A. D. Bandrauk, Phys. Rev. A **54**, 3254 (1996).
[33] S. Chelkowski and A. D. Bandrauk, Phys. Rev. A **65**, 061802 (2002).
[34] J. Garza, R. Vargas, J. A. Nichols, and D. A. Dixon, J. Chem. Phys. **114**, 639 (2001).
[35] R. N. Barnett, U. Landmann, A. Nitzan, and G. Rajagopal, J. Chem. Phys. **94**, 608 (1991).
[36] A. D. Bandrauk and H. Yu, J. Phys. B **31**, 4243 (1999); Phys. Rev. A **59**, 539 (1999).
[37] F. Calvayrac, P.-G. Reinhard, and E. Suraud, J. Phys. B **31**, 5023 (1998).